Received: 10 March 2019 | Revised: 17 April 2019 | Accepted: 18 April 2019

DOI: 10.1111/jace.16522



Journal of the American Ceramic Society

ORIGINAL ARTICLE

# Tuning oxygen vacancy in $LiNbO_3$ single crystals for prominent memristive and dielectric behaviors



**Chunchang Wang**[1,2] | **Jie Sun**[1] | **Wei Ni**[1] | **Binbin Yue**[3,4] | **Fang Hong**[3,4] | **Hong Liu**[5] | **Zhenxiang Cheng**[1,6]

[1]Laboratory of Dielectric Functional Materials, School of Physics & Material Science, Anhui University, Hefei, P. R. China

[2]State Key Laboratory of Low-Dimensional Quantum Physics, Department of Physics, Tsinghua University, Beijing, People's Republic of China

[3]Center for High Pressure Science and Technology Advanced Research, Pudong, Shanghai, China

[4]Advanced Light Source, Lawrence Berkeley National Laboratory, Berkeley, California

[5]Institute for Advanced Interdisciplinary Research (IAIR), University of Jinan, Shandong, China

[6]Institute for Superconducting and Electronic Materials, University of Wollongong, North Wollongong, New South Wales, Australia

**Correspondence**
Chunchang Wang and Zhenxiang Cheng, Laboratory of Dielectric Functional Materials, School of Physics & Material Science, Anhui University, Hefei 230601, P. R. China.
Emails: ccwang@ahu.edu.cn (C. W.) and cheng@uow.edu.au (Z. C.)

**Funding information**
National Natural Science Foundation of China, Grant/Award Number: 51872001 and 51502001

**Abstract**

Understanding and manipulating the behavior of oxygen vacancy in oxide materials are of vital importance for rejuvenating materials with novel functionalities. We herein report a exciting phenomenon of oxygen vacancies changing from an isolated state to a clustered state in $LiNbO_3$ single crystals. The clustering of the oxygen vacancies induces a relaxor-like dielectric anomaly and a first-order phase transition. The relaxor-like dielectric anomaly was argued to be a pseudo-relaxor behavior resulting from the combined contributions of a dipolar relaxation and a Maxwell-Wagner relaxation. The first-order phase transition was ascribed to be an electric-ferroelectric phase transition. Interestingly, a well-defined melting point of the oxygen-vacancy clusters was observed. At temperatures near the point, a small dc field can lead to resistance switching from a high resistance state to a low resistance state, yielding a prominent memristive effect with the OFF/ON ratio of $10^2$. Our results underscore that controlling the oxygen vacancy state is a promising strategy to tailor the properties of oxides for novel device applications.

**KEYWORDS**

dielectric properties, $LiNbO_3$ single crystal, memristive effect, oxygen vacancy, phase transition

## 1 | INTRODUCTION

It is well-known that a native defect, oxygen vacancy ($V_O$), plays a decisive role in controlling the properties of oxides.[1] Our fundamental knowledge about how the $V_O$s work in oxides, in fact, is still at a nascent stage. It has been generally assumed that the $V_O$s behave as isolated particles without interactions. However, increasing theoretical evidences suggest that, when the concentration of $V_O$s is high enough, the vacancies will interact with each other forming an ordered state—$V_O$ clusters.[2,3] As a result, the $V_O$s show collective behavior rather than individual behavior. It is naturally expected

  

that the $V_O$ clusters would result in novel properties as compared with the isolated vacancies. Since the $V_O$s are virtually donors, when they aggregate into clusters, this would lead to electrical inhomogeneity in the material. Hence, the anticipation of novel dielectric and electric behavior raises interesting issues.

To gain insight into these issues, lithium niobate ($LiNbO_3$) single crystals were selected as model samples. $LiNbO_3$ crystal was selected for this study because it exhibits rich physical properties, such as electro-optic, acousto-optic, photoelastic, photorefractive, and photovoltaic effects, as well as ferro-, pyro-, and piezoelectric properties, which make it a multifunctional material.[4] It has been widely reported that both intrinsic and extrinsic point defects have a remarkable influence on these effects and properties.[5,6] Among them, the intrinsic point defects, such as Li, Nb, and O vacancies, lead to nonstoichiometry, which significantly changes the properties of $LiNbO_3$.[7] Therefore, a comprehensive knowledge of the point defects is the key requisite for better understanding and control of the properties of $LiNbO_3$. In the earlier literature, the oxygen-vacancy model was widely used to explain the conductivity and photogalvanic properties of $LiNbO_3$.[8–10] Later, this model was discarded because theoretical results revealed that the formation of cation vacancies, rather than oxygen vacancies, in $LiNbO_3$ is energetically favorable.[11–14] Recent results have shown that oxygen vacancy plays a decisive role in the magnetism, magnetocapacitance, and memristive behavior in $LiNbO_3$.[15–17]

The above background indicates that the role of oxygen vacancy in $LiNbO_3$ has not been fully understood. It is well known that low frequency (below 1 MHz) dielectric spectroscopy might be a powerful technique to investigate the dynamic behavior of point defects.[18] Although a wealth of dielectric studies related to $LiNbO_3$ ceramics, single crystals, and composites have been reported,[7,19–25] there are few reports on the effects of oxygen vacancies on the dielectric properties of $LiNbO_3$ crystals. It was the purpose of this work to explore the role played by oxygen vacancies in the dielectric and electric properties of $LiNbO_3$. Our results revealed that oxygen vacancies change from an isolated state to a clustered state when their concentration is high enough. The clustered state induces a phase-transition-like dielectric anomaly, a first-order phase transition, and a prominent resistance switching effect.

## 2 | EXPERIMENTAL PROCEDURES

All the $LiNbO_3$ (LN) crystal samples used in the present study were grown from the congruent melt by the Czochralski technique. Colorless transparent (104) LN wafers were cut from large single-crystal boules (see Figure S1). These wafers are usually referred to as "congruent lithium niobate (CLN)" wafers. In order to tune the oxygen vacancy level, the CLN wafers were buried in a mixture of iron and lithium carbonate ($Fe:Li_2CO_3$ = 5:100 by mass) and held in a muffle furnace at different temperatures in the range of 450°C–550°C under flowing nitrogen gas. The reduction process involved heating the samples to the desired temperature, holding them for 6 hours and then slowly cooling down to room temperature. After chemical reduction, the color of the samples changed, from grey to black and almost opaque, depending on the treatment temperature. Grey lithium niobate wafers were obtained at 460°C and are denoted as "GLN" wafers. Likewise, black lithium niobate wafers were obtained at 540°C and are denoted as "BLN" wafers [see the inset of Figure S1].

Phase purity of the crystal wafers was characterized by X-ray powder diffraction (XRD) performed on a Rigaku SmartLab diffractometer (Rigaku Beijing Co., Beijing, China) with Cu$K_\alpha$ radiation. X-ray photoelectron spectroscopy (XPS, Thermo-Fisher ESCALAB 250Xi) was used to analyze the valence state of O element. The concentration of oxygen vacancies was found to increase as the colour of the crystal became darker (see Figure S2). Differential scanning calorimetry (DSC) measurements were carried out with a PE Pyres-1 DSC apparatus at a heating rate of 10°C/min. Dielectric properties were measured using a Wayne Kerr 6500B precise impedance analyzer (Wayne Kerr Electronic Instrument Co., Shenzhen, China) with the sample mounted in a holder placed inside a PST-2000HL dielectric measuring system (Partulab Co., Wuhan, China). The ac measurement signal was 100 mV. Electrodes were made by printing silver paste on both sides of the disk-type samples. The synchrotron X-ray Laue diffraction experiments were performed at Beamline 12.3.2 in the Advanced Light Source of the Lawrence Berkeley National Laboratory, Berkeley, California. The polychromatic beam energy ranged from 6 to 22 keV. A one micron beam was obtained via a Kirkpatrick-Baez (KB) mirror. A silicon single crystal was used for calibration to precisely determine the experimental geometry such as the sample-to-detector distance. The sample was placed on an Anton-Paar DHS 900 heating stage, and the patterns were collected at several temperatures between ambient and 600°C. The current-voltage characteristics were collected using a Keithley 2400 SourceMeter.

## 3 | RESULTS AND DISCUSSIONS

Figure 1 summarizes the temperature (T) dependence of the dielectric properties for the CLN (A-C), GLN (D-F), and BLN (G-I) crystals. The curves recorded at the frequencies of $10^2$, $10^3$, $10^4$, $10^5$, $5 \times 10^5$, and $10^6$ Hz were selected to be shown in the figure. It is seen that the dielectric constant, $\varepsilon'(T)$, of the CLN initially exhibits a slight increase followed

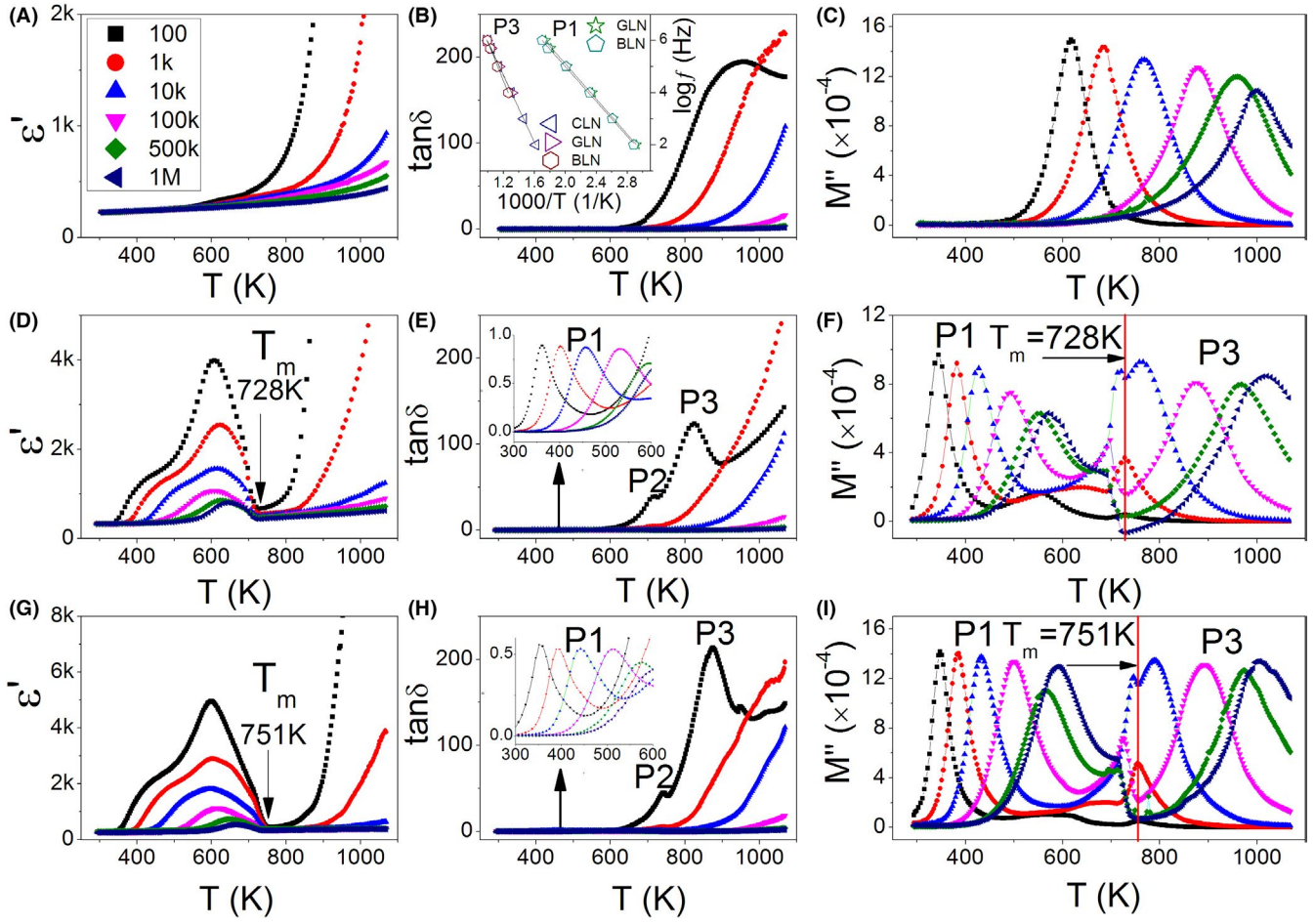


**FIGURE 1** Temperature dependence of dielectric properties for the CLN (A-C), GLN (D-F), and BLN (G-I). The inset in (B) is the Arrhenius plots for the relaxations P1 and P3 found in CLN, GLN, and BLN. The straight lines are linear fitting results. The insets in (E) and (H) are enlarged view of the low-temperature range. The vertical lines in (F) and (I) indicate the melting point of the oxygen-vacancy clusters [Color figure can be viewed at wileyonlinelibrary.com]

by a rapid increase around 800 K (Figure 1A). Meanwhile, a pronounced loss tangent [tan$\delta(T)$] peak corresponding to the rapid increase is found (Figure 1B). This fact indicates that there is a relaxation process in CLN. The relaxation peak can be only observed in the tan$\delta(T)$ curve measured at 100 Hz, whereas the peaks in the curves measured at frequencies higher than 100 Hz move towards higher temperatures beyond the tested temperature window. This prevents us from obtaining the relaxation parameters. To shed light on this relaxation, the dielectric function of electric modulus, defined as $M^* = M' + jM'' = 1/\varepsilon^*$, is applied. It was reported that the relaxation time for the electric modulus ($\tau_M$) is lower than that of the dielectric loss tangent ($\tau_\delta$), $\tau_M < \tau_\delta$.[26] Therefore, compared with the dielectric loss tangent, the relaxation should occur at a lower temperature in the spectra of the electric modulus. Figure 1C displays the temperature dependence of the imaginary part of the electric modulus for the CLN, from which a set of relaxation peaks can be clearly seen. The measurement frequency ($f$) was plotted as a function of the reciprocal of the peak position ($T_P$) according to the Arrhenius law:

$$f = f_0 \exp\left(-E_a/k_B T_P\right) \quad (1)$$

where $f_0$ is the prefactor, $E_a$ is the activation energy of the relaxation, and $k_B$ is the Boltzmann constant. The Arrhenius plot of the relaxation is shown in the inset of Figure 1B. A linear fit yields the relaxation parameters $f_0 = 2.36 \times 10^{12}$ Hz and $E_a = 1.28$ eV. The activation energy value locates in the range of ~1.0 to 1.5 eV for the relaxation caused by hopping motion of individual oxygen vacancies,[27–29] indicating that the relaxation might be related to oxygen vacancies.

The crystals of GLN and BLN show similar dielectric behavior, that is, $\varepsilon'(T)$ exhibits a broad anomaly, which is composed of a step-like increase followed by a relaxor-like peak. The peaks recorded at different frequencies converge to a well-defined temperature ~$T_m$728 K for GLN and ~751 K for BLN as indicated by the arrows in Figure 1D,G, respectively. In the temperature range above $T_m$, $\varepsilon'(T)$ for both crystals rapidly increases with increasing temperature, showing the same behavior as that of the CLN. In the tanδ ($T$) curves, there is a set of relaxation

peaks (P1) corresponding to the step-like increase in $\varepsilon'(T)$ [see the enlarged plots of the low-temperature range of tanδ ($T$) curves shown as insets in Figure 1E,H]. The Arrhenius plots of P1 [inset of Figure 1B] yield the relaxation parameters $f_0 = 5.21 \times 10^{11}$ Hz and $E_a = 0.68$ eV for GLN, and $f_0 = 3.18 \times 10^{11}$ Hz and $E_a = 0.67$ eV for BLN. The activation energy for both crystals is very close to the typical value of ~ 0.70 eV for the relaxation associated with oxygen-vacancy clusters.[27,30,31] The migration of an isolated vacancy is fulfilled via hopping motion. The relaxation related to the isolated vacancy is composed of two contributions: $E_a+E_G+E_H$, with $E_G$ and $E_H$ being the defect generation and hopping energies, respectively. Whereas for the clusters, lattice distortions induced by the oxygen vacancies will overlap, leading to the formation of defect band in the band gap.[32] The hopping motion then transforms to band conduction. The relaxation related to the clustered vacancies is solely determined by $E_G$. Therefore, a remarkable decrease in the activation energy occurs when the oxygen vacancies condense into clusters. This finding strongly supports the theoretical prediction that a high oxygen vacancy concentration would lead to interaction of the oxygen vacancies with each other so as to form an ordered state,[2,33] and demonstrates that the anomaly is related to oxygen vacancies.

An oxygen-vacancy-related dielectric anomaly has been widely reported in oxides at high enough temperatures.[34] This behavior is now called pseudo-relaxor behavior,[34] which is composed of two close relaxations, with the low temperature one being a dipolar relaxation and the high temperature one being a Maxwell-Wagner relaxation.[35] Although the two relaxations are not observed in the tanδ($T$) curves in the anomaly temperature range, they can be well-identified in the modulus spectra (see Figure 1F,I). For clarification, the modulus spectra recorded at 100 Hz for the GLN and BLN are presented in Figure S3 of the Supporting Information. From which, one can clearly see that the second relaxation peak (P1′) occurs at 553 K for GLN and 562 K for BLN. The Maxwell-Wagner nature of the P1′ peak is confirmed by the impedance measurements under different dc biases as seen in Figure S4. This finding leads to the conclusion that the anomaly found in GLN and BLN is the so-called pseudo-relaxor behavior caused by Maxwell-Wagner relaxation. Since the Maxwell-Wagner relaxation is linked to the kind of interface, a pertinent question is what kind of interface exists in the present crystal? The ferroelectric domain walls and sample-electrode contacts can be excluded because both of them exist in CLN, which, however, shows no detectable dielectric anomalies. A tentative explanation for the anomaly is that the oxygen vacancies form an ordered phase. It is the phase boundary between the cluster phase and the matrix phase that leads to the Maxwell-Wagner relaxation. When the measurement temperature is high enough, the escaping of the vacancies from the cluster phase becomes notable. It

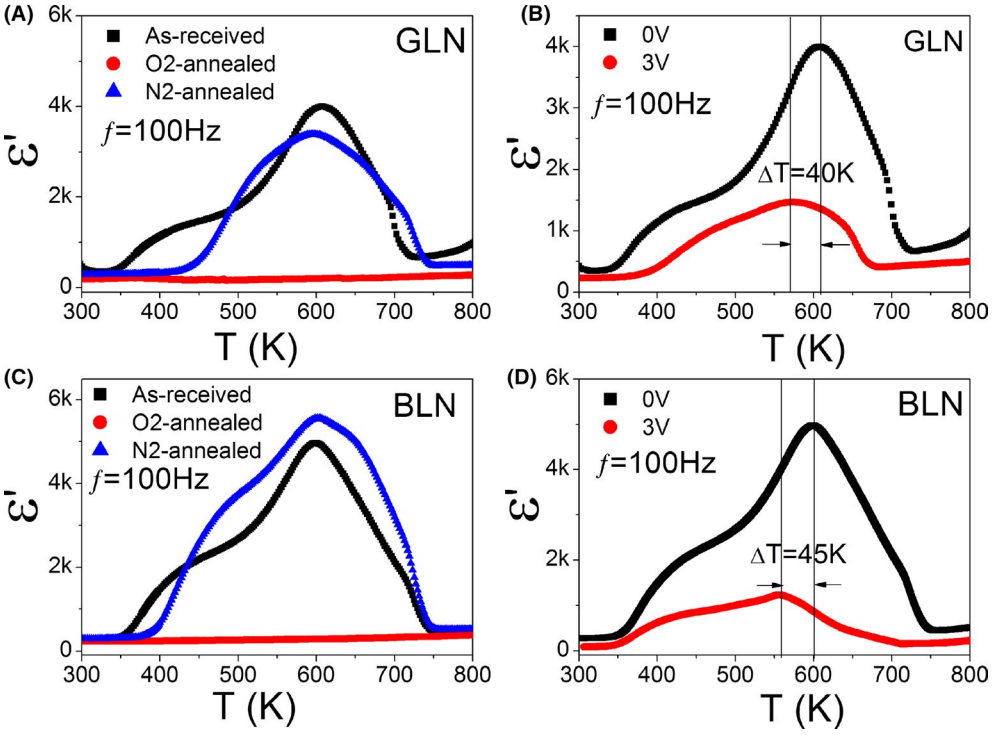


**FIGURE 2** Comparison of the temperature dependence of the dielectric constant for GLN (A) and BLN (B) in the as-received, $O_2$-annealed, and $N_2$-annealed cases. Temperature dependence of the dielectric constant for GLN (A) and BLN (B) measured without and with a dc bias of 3 V [Color figure can be viewed at wileyonlinelibrary.com]

is natural to expect a critical temperature, $T_m$, at which the oxygen-vacancy cluster phase may be "de-clustered" because the interaction energy of the vacancies cannot resist the thermal fluctuation. The $T_m$ is actually the "melting point" of the clusters. In the temperature range higher than $T_m$, the vacancies exhibit individual behavior, and their hopping motions yield a relaxation with an activation energy around 1.0 eV or higher.

To substantially corroborate the relationship between the oxygen vacancies and the observed dielectric anomaly, crystals of GLN and BLN were subjected to two consecutive post-annealing treatments: first in oxygen and then in nitrogen atmosphere (both with purity >99.99% and a flow rate of 200 mL $min^{-1}$) at 1073 K for 2 hours. After each treatment, the dielectric properties were measured as a function of temperature. Figure 2A,B compares the temperature dependence of the dielectric constant (obtained at 100 Hz) for the GLN and BLN, respectively, in the as-received, $O_2$-annealed, and $N_2$-annealed cases. It is clearly seen that the step-like increase and the relaxor-like anomaly for both crystals disappear completely after the $O_2$-annealing treatment and reappear after the $N_2$-annealing treatment. This result unambiguously confirms that both the step-like increase and the relaxor-like anomaly are associated with oxygen vacancies.

It is noteworthy that there are two visible tan$\delta$ peaks (P2 and P3) in GLN and BLN occurring in the temperature range above that of the P1 peak. These peaks can be identified in the curves measured at low frequencies, for example, 100 Hz. A detailed investigation of $\varepsilon'(T)$ at lower frequencies ($<10^3$ Hz) reveals that P2 is a phase-transition-type peak (because the peak position is independent of the measurement frequency) and P3 is a relaxation-type peak (see Figure S5). The transition temperature ($T_C$) is found to be 715 K for GLN and 740 K for BLN. Both occur in the temperature range below $T_m$, where the oxygen-vacancy-ordering dominates the dielectric properties of the crystal. Similar to what was found in $Na_{0.5}Bi_{0.5}Cu_3Ti_4O_{12}$,[36] the ordering of oxygen vacancies may incur the ferroelectric phase transition. This kind of ferroelectricity is now named as "electric ferroelectricity", which is almost a common dielectric phenomenon in transition-metal oxides occurring at high enough temperatures. Instead of *a change in crystal structure*, the mechanism of such ferroelectric behavior involves *a change in electronic structure* that breaks the space-inversion symmetry giving rise to a macroscopic polarization.[33,37] Therefore, the P2 peak can be reasonably ascribed to an electric-ferroelectric phase transition. The relaxation-type P3 peak appears in the temperature range higher than $T_m$ and can be clearly seen in the modulus spectra (see Figure 1F,I).

Due to the phase transition, the peak of P1′ is strongly disturbed. The range of the disturbance is from $T_C$ to $T_m$. This interference prevents us from deducing the relaxation parameters of P1′. We therefore focus on calculating the relaxation parameters of P1 and P3 from the modulus spectra. Arrhenius plots for P1 and P3 are shown in the inset of Figure 1B. The relaxation parameters were calculated, and the results are given in Table S1 of the Supporting Information. From this table, we can see that the relaxation parameters of P3 agree well with those of CLN, indicating that the dielectric behavior of GLN and BLN in the temperature range of $T \geq T_m$ is dominated by individual oxygen vacancies. The relaxation parameters of the P1 peak for GLN and BLN agree well with those deduced from the tan$\delta$ ($T$) curves, indicating that the dielectric behavior of GLN and BLN in the temperature range of $T < T_C$ is associated with the clustered state of oxygen vacancies. In other words, the oxygen vacancies show collective behavior in this temperature range. The oxygen-vacancy ordering scenario is firmly supported by the results of thermal analysis (see Figure S6 of the), which clearly reveal a well-defined endothermic peak at ~432 K for BLN. This peak becomes broader and much weaker in GLN and invisible in CLN. This finding clearly demonstrates that (a) the oxygen vacancies in GLN and BLN undergo a redistribution process from an ordered state to a disordered state, that is, the cluster melting process, (b) no clustered state exists in CLN, that is, the vacancies therein are in an isolated state, and (c) the clustered state becomes notable with increasing oxygen-vacancy concentration. It is worth pointing out that the phase transition temperature deduced from the DSC results is lower than that deduced from the dielectric results. This is because that the phase transition temperature of a clustered system is strong size-dependent.[38] The DSC measurement requires the bulk crystal to be ground into powders. The reduction in sample size leads to the decrease in the phase transition temperature.

The ordering of oxygen vacancies has been reported in a few oxides to have a preferential direction.[39] However, the in situ synchrotron Laue x-ray diffraction studies on the BLN recorded at a series of temperatures reveal no extra diffraction spots (see Figure S7). This fact indicates that the vacancies in the present crystals just condense into clusters without a long-range order.

In view of the above discussion, it is instructive to modulate the clustered state by a dc bias, as the motion of oxygen vacancies can be both thermally activated and electrically activated. A dc field is expected to promote the migration of the vacancies, which is beneficial to the formation and/or growth of the clusters. The dielectric constant curves as a function of temperature without and with a dc bias of 3 V for GLN and BLN are presented in Figure 2C,D, respectively. One can clearly see that the dc bias shifts the anomaly peak by 40 K for GLN and 45 K for BLN towards lower temperature. This result confirms that the dc field is favorable for the clustered state. On the other hand, the peak intensity for both crystals was greatly depressed by the bias. This is because the Maxwell-Wagner relaxation is usually associated with a Schottky barrier that can be depressed by dc bias.[40]

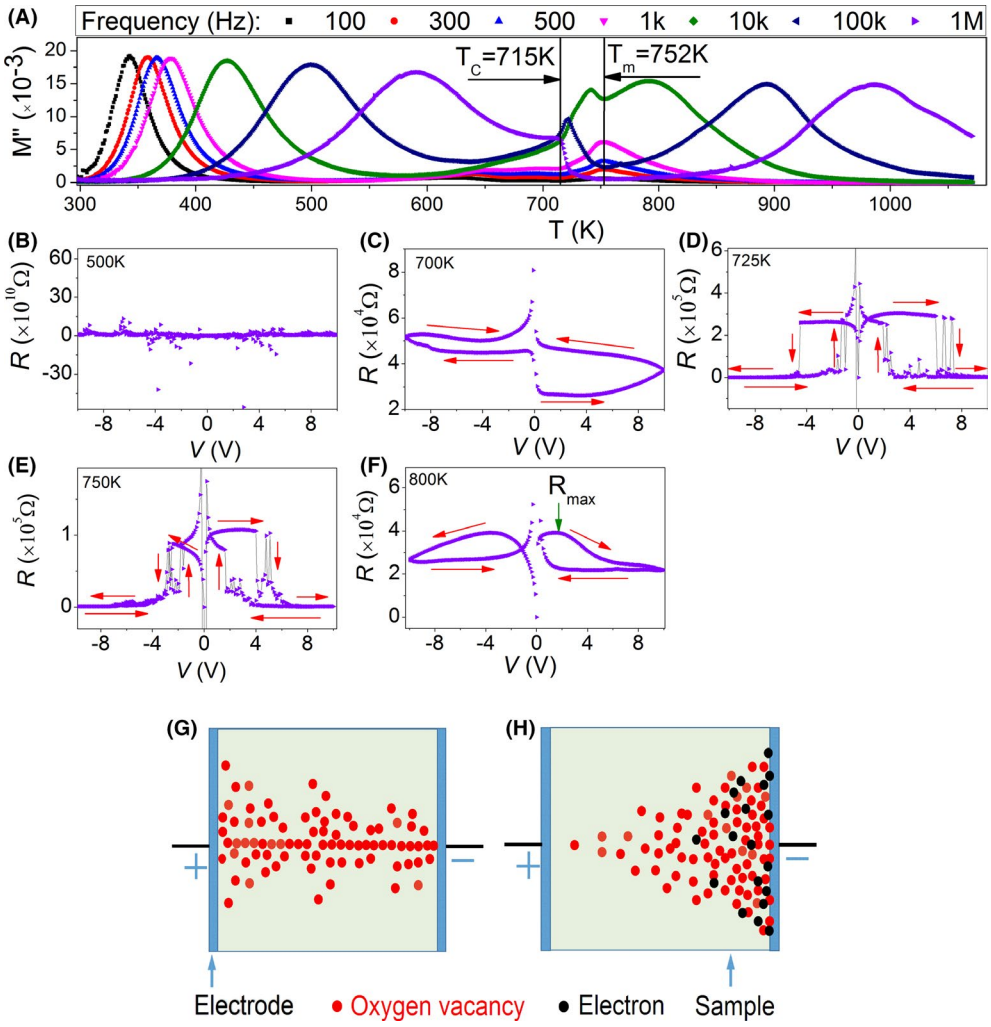


**FIGURE 3** (A) Temperature dependence of the electric modulus of the GLN from another batch of crystals. (B-F) The calculated resistance as a function of voltage for the selected temperatures. (G-H) Schematic illustration showing the overlapping state of the oxygen-vacancy clusters (G) and the melted state (H) [Color figure can be viewed at wileyonlinelibrary.com]

As a small dc field is found to be helpful for the formation and/or growth of the clusters, one would intuitively anticipate that, when the clusters become large enough, they can merge into a bigger one and contact with the electrodes forming a conductive filament. In this case, a memristive/resistive switching effect should be observed. To gain more insight, current-voltage (*I-V*) curves of the GLN were collected from another batch of crystals at different temperatures by sweeping the voltage in the sequence of 0→10→0→-10→0 V. The crystal shows $T_C$ and $T_m$ of 715 and 752 K, respectively (Figure 3A). The calculated resistance (*R*) values as a function of voltage at selected temperatures are shown in Figure 3B-F. It was found that the resistance is almost independent of the dc bias in the temperature range below 550 K [Figure 3(B)]. This is because that the $V_O$s in this range are in the clustered state, few residual isolated vacancies can be driven by the dc field and contribute to the conductivity. Meanwhile, the clusters themselves are almost "frozen," and "hard" enough to be deformed by the applied field, thereby making negligible contribution to the conductivity. At temperatures near $T_C$, for example, 700 K, the cluster growth from oxygen vacancy migration becomes notable. This process yields much smaller values of *R* compared to the frozen cluster state. At high biases, the cluster growth tends to be finished. The resistance then greatly increases with increasing bias, giving rise to a low resistance state (LRS or ON) in the forward branch (increasing bias) and a high resistance state (HRS or OFF) in the backward branch (decreasing bias) for both positive and negative biases (Figure 3C). In the temperature range between $T_C$ and $T_m$, the clusters become "soft," they can be easily elongated by the applied field. As illustrated in Figure 3G, when several elongated clusters overlap each other, a conductive filament is generated, which leads to an abrupt resistance switching from the HRS to the LRS (Figure 3D,E). The resistance switching voltage in the forward branch was found to be ~6 V at 725 K. In the backward branch, the opposite effect, that is, the LRS jumping to the HRS is observed. Due to the inertia

of the vacancies, the jumping voltage was found to occur at the lower value of ~2.2 V. A prominent resistance OFF/ON ratio of ~$2 \times 10^2$ at 725 K and $1.3 \times 10^2$ at 750 K were achieved. Similar behavior was found in the negative bias side. In the temperature range higher than $T_m$, the clusters are melted, and the vacancies are in an isolated state. The isolated vacancies can be moved by the field, and they will finally accumulate near the cathode because the electrode cannot conduct ions. The accumulated vacancies will create an internal field opposite to the field of the dc bias, which prevents more vacancies from moving towards the cathode. As a result, the resistance increases with increasing bias until the electrons at the cathode overcome the barrier and are injected into the sample [as depicted in Figure 3H]. The injected electrons will weaken the internal field and thus the resistance in the high-bias range decreases with increasing bias, yielding a $R_{max}$ in the forward branch as indicated by the olive arrow. In the backward branch, due to the inertia of the vacancies, the resistance goes along a curve with lower resistance values than those of the forward branch, which gives rise to a clockwise loop (Figure 3F).

It is important to emphasize that the memristive effect in $LiNbO_3$ single crystals induced by the melting of oxygen-vacancy clusters obviates a high-field electron-forming step and can be achieved at a small field on the order of ~10 V/cm. If this prominent memristive effect could be shifted to temperatures around room temperature, it would be very exciting for device implementation, which still awaits numerous further efforts.

## 4 | CONCLUSIONS

In summary, we demonstrate that $V_O$s in $LiNbO_3$ single crystals change from an isolated state to a clustered state with increasing the concentration of $V_O$s. A relaxor-like dielectric anomaly and a first-order phase transition were induced by the $V_O$ clustering. The relaxor-like dielectric anomaly was argued to be a pseudo-relaxor behavior and the first-order phase transition was related to be an electric-ferroelectric phase transition. A prominent memristive effect was found in the temperature range close to the melting point of the clusters. This effect is ascribed to the formation of a conductive filament under a small dc field.

## ACKNOWLEDGMENTS

The authors acknowledge the financial support from the National Natural Science Foundation of China (Grant Nos. 51872001 and 51502001). This work was supported in part by the Open Research Fund Program of the State Key Laboratory of Low-Dimensional Quantum Physics (Grant No. KF201803). ZX. Cheng thanks Australia Research Council (ARC) for support. BB. Yue and F. Hong acknowledge the support from the NSAF (Grant No. U1530402). This research used resources of the Advanced Light Source, which is a DOE Office of Science User Facility under contract no. DEAC02-05CH11231. The authors acknowledge the support from Dr. Nobumichi Tamura and Dr. Camelia Stan during the high temperature Laue-diffraction experiments at BL 12.3.2 of ALS/LBNL.

## ORCID

*Chunchang Wang* https://orcid.org/0000-0002-2349-1098

*Jie Sun* https://orcid.org/0000-0002-3230-4012

## REFERENCES

1. Kim HS, Cook JB, Lin H, Ko JS, Tolbert SH, Ozolins V, et al. Oxygen vacancies enhance pseudocapacitive charge storage properties of $MoO_{3-x}$. Nat Mater. 2017;16(4):454–60.
2. Marrocchelli D, Madden PA, Norberg ST, Hull S. Structural disorder in doped zirconias, part II: vacancy ordering effects and the conductivity maximum. Chem Mater. 2011;23(6):1365–73.
3. Cuong DD, Lee B, Choi KM, Ahn HS, Han S, Lee J. Oxygen vacancy clustering and electron localization in oxygen-deficient $SrTiO_3$: LDA + U study. Phys Rev Lett. 2007;98(11):115503.
4. Sando D, Jaatinen E, Devaux F. Reversal of degradation of information masks in lithium niobate. Appl Opt. 2009;48(24):4676–82.
5. Lorenzo A, Jaffrezie H, Roux B, Boulon G, García-Solé J. Lattice location of rare-earth ions in $LiNbO_3$. Appl Phys Lett. 1995;67:3735–7.
6. Malovichko G, Grachev V, Kokanyan E, Schirmer O. Axial and low-symmetry centers of trivalent impurities in lithium niobate: chromium in congruent and stoichiometric crystals. Phys Rev B. 1999;59(14):9113–25.
7. Xue D, Kitamura K. Dielectric characterization of the defect concentration in lithium niobate single crystals. Solid State Commun. 2002;122(10):537–41.
8. Jorgensen PJ, Bartlett RW. High temperature transport processes in lithium niobate. J Phys Chem Solids. 1969;30(12):2639–48.
9. Papazian KZ, Kalantarian AH, Vardanian RA. On optical and photoelectric properties of the $LiNbO_3$: Fe compounds. Ferroelectrics. 1996;188(1):157–73.
10. Fay H, Alford WJ, Dess HM. Dependence of second-harmonic phase-matching temperature in $LiNbO_3$ crystals on melt composition. Appl Phys Lett. 1968;12(3):89–92.
11. Schirmer OF, Thiemann O, Wöhlecke M. Defects in $LiNbO_3$—I. Experimental aspects. J Phys Chem Solids. 1991;52(1):185–200.
12. Donnerberg H, Tomlinson SM, Catlow CR, Schirmer OF. Computer-simulation studies of intrinsic defects in $LiNbO_3$ crystals. Phys Rev B Condens Matter. 1989;40(17):11909–16.
13. DeLeo GG, Dobson JL, Masters MF, Bonjack LH. Electronic structure of an oxygen vacancy in lithium niobate. Phys Rev B Condens Matter. 1988;37(14):8394–400.
14. Li Q, Wang B, Woo CH, Wang H, Wang R. First-principles study on the formation energies of intrinsic defects in $LiNbO_3$. J Phys Chem Solids. 2007;68(7):1336–40.

15. Díaz-Moreno Ca, Farías-Mancilla R, Matutes-Aquino Ja, Elizalde-Galindo J, Espinosa-Magaña F, González-Hernández J, et al. Magnetic behavior in $LiNbO_3$ nanocrystallites caused by oxygen vacancies. J Magn Magn Mater. 2014;356:82–6.
16. Díaz-Moreno C, Lopez J, González-Hernández J, Escudero R, Heiras JL, Yacamán MJ, et al. Magnetocapacitance effect in ferromagnetic $LiNbO_3$ nanoparticles. J Magn Magn Mater. 2016;407:291–8.
17. Li H, Xia Y, Xu B, Guo H, Yin J, Liu Z. Memristive behaviors of $LiNbO_3$ ferroelectric diodes. Appl Phys Lett. 2010;97(1):012902.
18. Zhu M, Zhang N, Wang H, Li YD, Huang SG, Li QJ, et al. Point-defect-induced colossal dielectric behavior in GaAs single crystals. RSC Adv. 2017;7(42):26130–5.
19. Lanfredi S, Rodrigues ACM. Impedance spectroscopy study of the electrical conductivity and dielectric constant of polycrystalline $LiNbO_3$. J Appl Phys. 1999;86(4):2215–9.
20. Karapetyan KG, Kteyan AA, Vardanyan RA. Thermal reduction effect on Curie temperature of $LiNbO_3$ ferroelectrics. Solid State Commun. 2006;140(9):474–6.
21. Abdel-Khalek EK, Bahgat AA. Optical and dielectric properties of transparent glasses and nanocrystals of lithium niobate and lithium diborate in borate glasses. Physica B Condens Matter. 2010;405(8):1986–92.
22. Kim JE, Kim SJ, Ohshima K-I, Hwang YH, Yang YS. Crystallization and dielectric properties of $4LiNbO_3$–$SiO_2$ glass. Mater Sci Eng A. 2004;375–377:1255–8.
23. Nataf GF, Aktas O, Granzow T, Salje EK. Influence of defects and domain walls on dielectric and mechanical resonances in $LiNbO_3$. J Phys Condens Matter. 2016;28(1):015901.
24. Wang Q, Liu C, Gao Y, Ma Y, Han Y, Gao C. Mixed conduction and grain boundary effect in lithium niobate under high pressure. Appl Phys Lett. 2015;106(13):132902.
25. Han Y, Li L, Xia W, Liu Y, Ren X. Dielectric relaxation in $LiNbO_3$–$MgAl_2O_4$ nanocomposite. Mater Lett. 2012;83:94–6.
26. Gerhardt R. Impedance and dielectric spectroscopy revisited: distinguishing localized relaxation from long-range conductivity. J Phys Chem Solids. 1994;55(12):1491–506.
27. Wang CC, Lei CM, Wang GJ, Sun XH, Li T, Huang SG, et al. Oxygen-vacancy-related dielectric relaxations in $SrTiO_3$ at high temperatures. J Appl Phys. 2013;113(9):094103.
28. Shulman HS, Damjanovic D, Setter N. Niobium doping and dielectric anomalies in bismuth titanate. J Am Ceram Soc. 2000;83(3):528–32.
29. Ke Q, Lou X, Wang Y, Wang J. Oxygen-vacancy-related relaxation and scaling behaviors of $Bi_{0.9}La_{0.1}Fe_{0.98}Mg_{0.02}O_3$ ferroelectric thin films. Phys Rev B. 2010;83(3):528–32.
30. Li W, Chen K, Yao Y, Zhu J, Wang Y. Correlation among oxygen vacancies in bismuth titanate ferroelectric ceramics. Appl Phys Lett. 2004;85(20):4717–9.
31. Wang XF, Lu XM, Zhang C, Wu XB, Cai W, Peng S, et al. Oxygen-vacancy-related high-temperature dielectric relaxation in $SrTiO_3$ ceramics. J Appl Phys. 2010;107(11):114101.
32. Zhang J, Li Y, Xu DY, Tong L, Qi HC, Wang CC. Low-frequency dielectric properties of $SrLaAlO_4$ ceramics. Ceram Int. 2017;43(7):5467–70.
33. Burbano M, Norberg ST, Hull S, Eriksson SG, Marrocchelli D, Madden PA, et al. Oxygen vacancy ordering and the conductivity maximum in $Y_2O_3$-doped $CeO_2$. Chem Mater. 2012;24(1):222–9.
34. Wang CC, Dou SX. Pseudo-relaxor behaviour induced by Maxwell-Wagner relaxation. Solid State Commun. 2009;149(45):2017–20.
35. Wang CC, Zhang MN, Xu KB, Wang GJ. Origin of high-temperature relaxor-like behavior in $CaCu_3Ti_4O_{12}$. J Appl Phys. 2012;112(3):034109.
36. Wang C, Ni W, Sun X, Wang L, Wang C, Jin K. Relaxor-like behaviors in $Na_{1/2}Bi_{1/2}Cu_3Ti_4O_{12}$ ceramics. J Am Ceram Soc. 2017;100(5):2016–23.
37. Sagayama H, Toyoda S, Sugimoto K, Maeda Y, Yamada S, Arima T. Ferroelectricity driven by charge ordering in the A-site ordered perovskite manganite $SmBaMn_2O_6$. Phys Rev B. 2014;90(24):241113.
38. Berry RS, Smirnov BM. Phase transitions in various kinds of clusters. Phys Uspekhi. 2009;52(2):137–64.
39. Yamauchi K, Barone P. Electronic ferroelectricity induced by charge and orbital orderings. J Phys Condens Matter. 2014;26(10):103201.
40. Wang CC, He M, Yang F, Wen J, Liu GZ, Lu HB. Enhanced tunability due to interfacial polarization in $La_{0.7}Sr_{0.3}MnO_3$/$BaTiO_3$ multilayers. Appl Phys Lett. 2007;90(19):192904.

## SUPPORTING INFORMATION

Additional supporting information may be found online in the Supporting Information section at the end of the article.

**How to cite this article:** Wang C, Sun J, Ni W, et al. Tuning oxygen vacancy in $LiNbO_3$ single crystals for prominent memristive and dielectric behaviors. *J Am Ceram Soc*. 2019;102:6705–6712. https://doi.org/10.1111/jace.16522